Ultrasonics 98 (2019) 35–50

Contents lists available at ScienceDirect

Ultrasonics

journal homepage: www.elsevier.com/locate/ultras

# A tunable bidirectional SH wave transducer based on antiparallel thickness-shear ($d_{15}$) piezoelectric strips

Mingtong Chen[a,b], Qiang Huan[a,b], Zhongqing Su[c], Faxin Li[a,b,*]

[a] LTCS and College of Engineering, Peking University, Beijing 100871, China
[b] Center for Applied Physics and Technology, Peking University, Beijing, China
[c] Department of Mechanical Engineering, The Hong Kong Polytechnic University, Hung Hom, Kowloon, Hong Kong Special Administrative Region

ARTICLE INFO

*Keywords:*
Guided wave
Shear horizontal wave
Piezoelectric transducer
Thickness-shear
Electromagnetic acoustic transducer (EMAT)

ABSTRACT

Guided wave based defects inspection is very promising in the field of structural health monitoring (SHM) and nondestructive testing (NDT) due to its less dissipation and thus long distance coverage. In comparison with the widely used Lamb waves, shear horizontal (SH) waves are relatively simple but less investigated probably due to the traditional notion that SH waves were usually excited by electromagnetic acoustic transducers (EMAT). In this work, we proposed a tunable method to excite single-mode bidirectional SH waves in plates using antiparallel thickness-shear ($d_{15}$) piezoelectric strips (APS). The proposed SH wave driving mechanism here is similar to that by using the periodic permanent magnetics (PPM) based EMAT with the period of strips equal to half of the wavelength. Both finite element simulations and experiments were conducted to validate this transducer in excitation of bidirectional SH waves. Results show that the Lamb waves excited by single piezoelectric strip can be suppressed very well. The radiation angle of the excited bidirectional SH wave can be reduced by extending the strip length, increasing the driving frequency or using more strips. Moreover, the APS transducer can selectively excite $SH_1$ wave and suppress the $SH_0$ wave at 174 kHz and 273 kHz in a 10 mm-thick aluminum plate. Considering its simple structure, flexible design and low excitation energy, the APS SH wave transducer is expected to be widely used in near future.

## 1. Introduction

Ultrasonic guided wave had been more and more widely used in the field of nondestructive testing (NDT) and structural health monitoring (SHM) due to its less dissipation and thus long distance (large area) coverage [1–4]. In plate-like structures, both Lamb waves and shear horizontal (SH) waves can exist. SH waves only have one displacement component which is parallel to the plate surface and perpendicular to the wave propagation direction [5]. Theoretically, the wave modes of SH waves are much simpler than that of the Lamb waves. However, in practice, SH waves were less used than Lamb waves, probably due to the traditional notion that SH waves were usually excited by electromagnetic acoustic transducers (EMAT) which required high energy in excitation and signal amplification circuit in reception.

In late 1970s, Thompson and co-workers proposed two type of EMATs to excite SH waves in plates: one is composed of periodic permanent magnetics (PPM) based on the Lorentz force which applied for non-ferromagnetic metallic plates [6]; the other is based on in-plane magnetostriction which can only be used for ferromagnetic materials [7]. Kwun et al excited longitudinal, torsional and flexural wave modes in rods and pipes using magnetostrictive EMAT [8] and magnetostrictive patch transducers (MPT) [9], respectively, and found the latter is superior to the former. Kim et al proposed different configurations of MPTs for pipes and plates [10,11] and they also designed omni-directional SH wave MPTs for plate structures [12,13]. Ribichini et al. comparatively investigated the above-mentioned three types of EMATs in SH wave excitation/reception and concluded that both the PPM EMAT and MPT are superior to the magnetostrictive EMAT for steel plates [14]. Furthermore, the energy transfer efficiency the MPT is about one order higher than the PPM EMAT. Based on the PPM EMAT and MPT, some fundamental characteristics of SH waves had been experimentally studied [15,16] and SH wave based defect inspection in plates were conducted [17–19].

Actually, SH waves can also be excited by piezoelectrics. It is well known that a thickness-shear ($d_{15}$) piezoelectric transducer can excite SH waves perpendicular to its poling direction but simultaneously excite Lamb waves along the poling direction [20]. Recently, Boivin et al show that the Lamb waves can be well suppressed ($-16$ dB) at high

* Corresponding author at: LTCS and College of Engineering, Peking University, Beijing 100871, China.
*E-mail address:* lifaxin@pku.edu.cn (F. Li).

https://doi.org/10.1016/j.ultras.2019.06.001
Received 13 April 2019; Received in revised form 15 May 2019; Accepted 1 June 2019
Available online 03 June 2019
0041-624X/ 

drive frequency if the $d_{15}$ piezoelectric strip is very long [21]. Miao et al proposed that single-mode SH wave can be excited/received by face-shear ($d_{24}$) piezoelectric transducers [22] or the synthetic face-shear mode piezoelectric wafers [23]. Bi-directional SH waves can also be excited, using dual face-shear ($d_{24}$) piezoelectric wafers [24]. Omni-directional SH wave piezoelectric transducers were also developed, based on the synthetic circumferential poling using $d_{15}$ and $d_{24}$ piezoelectric wafers [25,26], or based on thickness-poled, thickness-shear piezoelectric rings [27,28]. Based on $d_{15}$ piezoelectric SH wave transducers, the interactions of SH wave with cracks were systematically investigated [29,30]. Thickness gauging of plate [31], defect inspection in bending plate [32] and composites [33], structural health monitoring of plates using sparse array [34] and phased array [35], were also conducted based different SH wave piezoelectric transducers. Recently, Li et al established a fully-coupled dynamic model for $SH_0$ wave excitation in plates using $d_{15}$ piezoelectric strips [36], which had been validated by both finite element simulations and experiments at tuning frequencies.

It should be noted that the conventional EMATs based on PPM or magnetostrictively coupled meander-coil are by default bi-directional SH wave transducers, which can focus the wave energy in a controlled radiation angle and thus very promising in excitation of circumferential SH waves in pipes [37,38], or studying the fundamental characteristics of SH waves [15,16]. Furthermore, the EMAT based SH wave transducers usually can selectively excite single-mode SH waves in large frequency-thickness-product plates [15,16,18], e.g., suppressing $SH_0$ wave and exciting single-mode $SH_1$ for tomography [18]. However, none of the above-mentioned piezoelectric SH wave transducers has the mode selective capacity.

In this work, we proposed that single-mode bi-directional SH waves can be excited by antiparallel shearing line forces and the line forces can be provided either by PPM EMAT or $d_{15}$ mode piezoelectric strips. Thus, a novel bi-directional SH wave transducer based on antiparallel $d_{15}$ piezoelectric strips (APS) is proposed. Firstly, the working principle of this bidirectional SH wave transducer is presented at Section 2. Then, in Section 3, finite element simulations were employed to predict the performances of the APS based SH wave transducers with different strip lengths, spacing and strip numbers. Later, experiments were conducted to examine the performances of the proposed transducer in Section 4. Discussions were presented in Section 5 and conclusions were summarized in Section 6. The proposed bi-directional piezoelectric SH wave transducer can be widely used in NDT/SHM and specially suitable for studying the fundamental properties of SH waves, such as reflection, refraction, mode conversion, etc.

## 2. Methods

### 2.1. Working principle

As shown in Fig. 1(a), an alternating shearing line force (with the frequency $f$) along the $x_2$ axis will excite largest SH waves in the $x_1$ direction and largest Lamb waves in the $x_2$ direction [5,39]. The radiation angle (2θ) of the excited SH waves and Lamb waves depend on the length ($L$) of the line force and the driving frequency, which can reach π for the point force case [40]. In the case of a pair of antiparallel alternating shearing force with the interval of $T$, as shown in Fig. 1(b), the Lamb waves in the lateral far field ($x_2$ direction) will diminish via destructive interference. Meanwhile, the SH wave in the $x_1$ direction with the wavelength (λ) of $2T$ will be strengthened via constructive interference. Thus bidirectional SH wave is expected to be excited by such a pair of alternating, antiparallel shearing line force. Actually, this is the principle of SH wave excitation using PPM EMAT in which the Lorentz force serves as the shearing line force [6]. Here we proposed that the alternating shearing line force can also be provided by using thickness-shear ($d_{15}$) piezoelectric strips conveniently driven by electric field. Furthermore, as the energy conversion efficiency of piezoelectric transducers is much higher than that of EMAT, one pair of antiparallel $d_{15}$ piezoelectric strips (APS) should be capable of exciting SH wave with enough amplitude. That is, the structure of the APS SH wave transducer would be much simpler than the PPM EMAT where several pairs of permanent magnetics are required to enhance the excitation energy.

The principle of SH wave mode selection of the APS transducer is similar to that of PPM EMAT. When the wavelength of $SH_1$ mode equals double wavelength of the $SH_0$ mode, and the strip interval equals the $SH_0$ wavelength, i.e., $\lambda_{SH1} = 2\lambda_{SH0}$, and $T = \frac{\lambda_{SH1}}{2} = \lambda_{SH0}$, the $SH_0$ mode will diminish via destructive interference and the $SH_1$ mode will be strengthened via constructive interference. The frequency-thickness product ($fd$) for this condition can be directly calculated from the following explicit phase velocity of SH waves:

$$c_p(fd) = \pm 2c_T \left\{ \frac{fd}{\sqrt{4(fd)^2 - n^2 c_T^2}} \right\} \tag{1}$$

where $c_T$ is the velocity of bulk shear wave, $n$ is the order of the SH mode.

Actually, as long as $T = n\lambda_{SH0} \neq m\lambda_{SH1}$ (where both $n$ and $m$ are integers), the $SH_0$ mode will diminish and only $SH_1$ mode will be excited.

Theoretically, when $T = \lambda_{SH1} = 1.5\lambda_{SH0}$, the $SH_1$ mode will diminish and $SH_0$ mode will be strengthened. However, in practice, it is rather difficult to suppress the dispersive $SH_1$ mode and excite single-mode $SH_0$ wave in large $fd$ waveguide. Thus, single-mode $SH_0$ wave was usually excited below the cut-off frequency of the $SH_1$ wave.

### 2.2. Finite element simulations

To analyze the wave radiation patterns and the bidirectivity of the APS transducers, a three-dimensional finite element model was constructed using the ANSYS software. The material parameters of the PZT-5H strips used in the simulations were listed in Table 1. An aluminum plate with the dimension of 400 × 400 × 1 $mm^3$ is used as waveguide and its density, Young's modulus, Poisson ratio are 2700 $kg/m^3$, 71 GPa and 0.33, respectively. The piezoelectric strips were modeled by SOLID 5 elements and the plate was modeled by SOLID 185 elements in the ANSYS software. The APS transducer was perfectly bonded at the center of the plate without bonding layers. It was driven by 20 V voltage signal (five-cycle Hanning windows-modulated sinusoid tone burst) and the radial displacement component $u_r$, tangential displacement component $u_\theta$, and out-of-plane displacements component $u_z$ were extracted at the distance (100 mm) from the center of the APS. The largest size of elements was set to be less than 1/15 of the shortest wavelength and the time step was set to be less than 1/20 of the central frequency of the drive signal.

### 2.3. Experimental

Experiments were performed to explore the bidirectivity and the mode selection capacity of the proposed APS transducer, respectively. The experimental setup was shown shown in Fig. 2. For the bidirectivity testing, a thin aluminum plate with dimensions of 1000 × 1000 × 1 $mm^3$ was employed as the waveguided and the APS transducer was bonded on the plate using 502 epoxy adhesive with the bonding layer thickness of less than 20 μm. The $d_{15}$ piezoelectric strips were fabricated by commercial PZT-5H piezoelectric ceramics (Baoding Hongsheng Ceramic Inc., Hebei, China) with different dimensions and the material properties were listed in Table 1. Two kinds of receivers were used in the experiment, one is the $d_{15}$ type sensor with the dimensions of 12 × 2 × 0.8 $mm^3$ for receiving SH wave, the other is the $d_{31}$ type sensor with the dimensions of 6 × 6 × 1 $mm^3$ for receiving Lamb waves. The $d_{15}$ type sensor were bonded at the distance of 650 mm from the excitation source and the $d_{31}$ type sensor were bonded

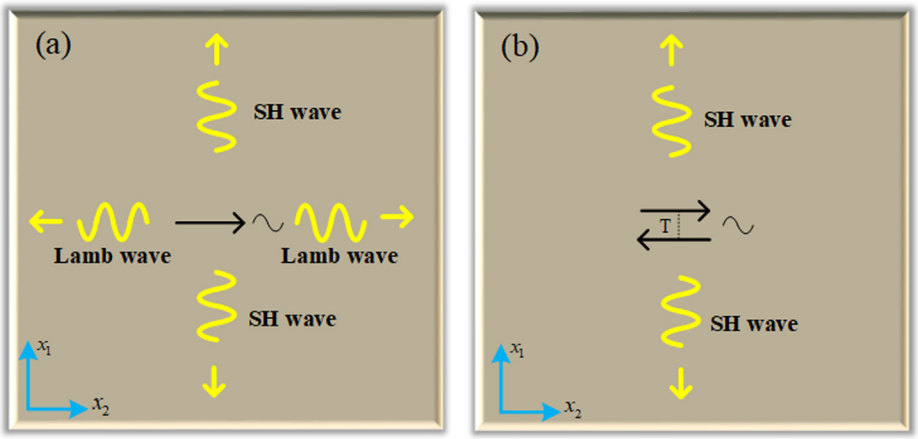


**Fig. 1.** The guided wave modes in a large plate generated by: (a) single shearing line force; (b) antiparallel shearing line force.

**Table 1**
Material properties of the PZT-5H piezoelectric strip used in the simulations.

| Density ($kg \cdot m^{-3}$) | Relative dielectric constant | | Piezoelectric constant ($pC \cdot N^{-1}$) | | |
|---|---|---|---|---|---|
| $\rho$ | $\varepsilon_{33}^X/\varepsilon_0$ | $\varepsilon_{11}^X/\varepsilon_0$ | $d_{33}$ | $d_{31} = d_{32}$ | $d_{15} = d_{24}$ |
| 7500 | 3400 | 3130 | 593 | −274 | 741 |
| Elastic compliances ($pm^2 \cdot N^{-1}$) | | | | | |
| $s_{11} = s_{22}$ | $s_{33}$ | $s_{12}$ | $s_{13} = s_{23}$ | $s_{44} = s_{55}$ | $s_{66}$ |
| 16.5 | 20.7 | −4.78 | −8.45 | 43.5 | 42.6 |

at the distance of 360 mm. For the mode selective SH wave excitation, a thick aluminum plate with dimensions of 1200 × 400 × 10 $mm^3$ was used to generate higher mode SH waves at relatively low frequency. The $d_{15}$ type sensors were also used in this experiment and it was 400 mm away from the excitation source. All the actuators were driven by five-cycle sinusoid tone-burst modulated into the Hanning window signal through a function generator (33220A, Agilent, USA). The driven signal was amplified by a power amplifier (7602 M, KROHN-HITE, USA) and the received signals were measured and collected by an oscilloscope (DSO-X 3024T, Agilent, USA).

## 3. Simulation results

We conducted a series of finite element simulations to examine the validity of the proposed bidirectional SH wave transducer based on antiparallel $d_{15}$ piezoelectric strips (APS). Firstly, in Sections 3.1 and 3.2, guided wave excitation by using single/antiparallel shearing line forces and $d_{15}$ piezoelectric strips were simulated, to check their differences in SH wave excitation. Then, in Sections 3.3 and 3.4, the effects of strip interval (or driving frequency) and strip numbers on suppressing the Lamb waves, grating lobes of SH wave and reducing the radiation angles, were systematically investigated. Due to the computational complexity using the ANSYS software, high frequency simulations were not conducted nor the mode selectivity of the proposed APS SH wave transducers. In Section 3.5, the performances of multiple piezoelectric strips in one row were also simulated in generating bidirectional SH waves. Finally, in Section 3.6, a simplified theoretical model was employed to predict the radiation pattern of the excited $SH_0$ wave and comparison were made between theoretical results and simulation results.

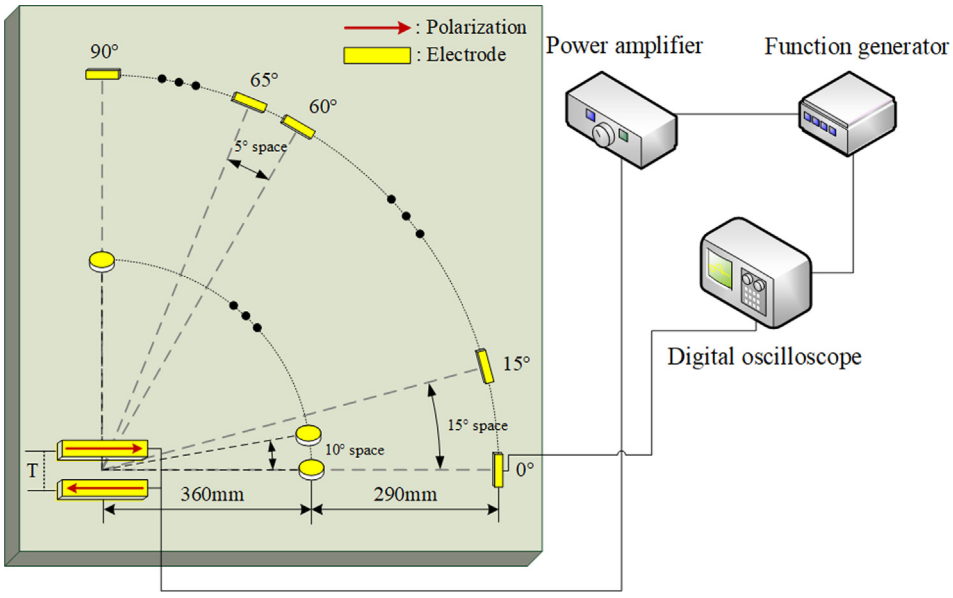


**Fig. 2.** Tesing setup for examining the performances of the proposed bidirectional SH wave transducer.

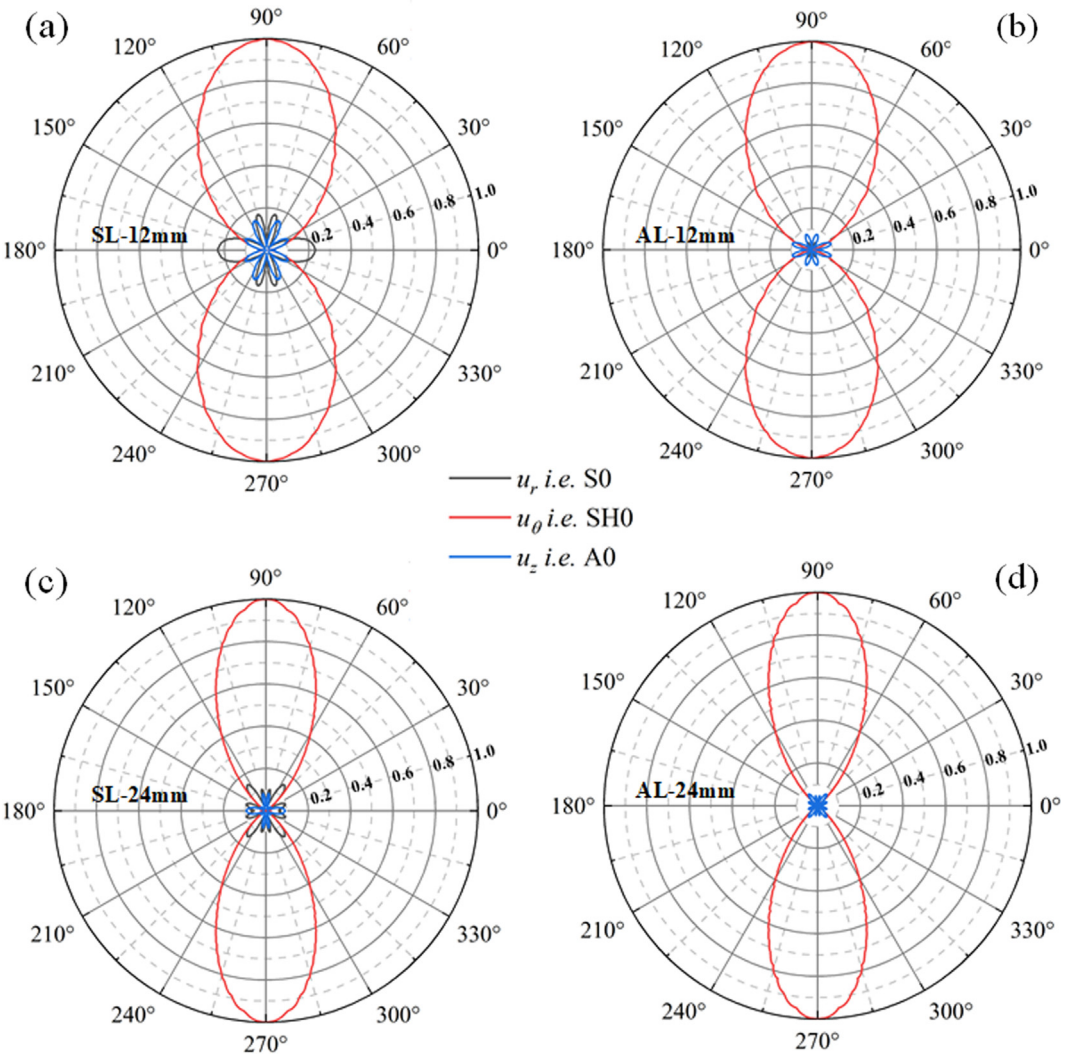


**Fig. 3.** Finite element simulated displacements of different guided wave modes generated in a 1 mm-thick aluminum plate at 196 kHz by using shearing line forces. Left: Single line force of (a) 12 mm length (SL-12 mm) and (c) 24 mm length (SL-24 mm); Right: Antiparallel line forces of (b) 12 mm length (AL-12 mm) and (d) 24 mm length (AL-24 mm). Interval between antiparallel line forces is 8 mm.

### *3.1. Guided wave excitations by using single and antiparallel shearing line forces*

Fig. 3 shows the simulated displacements of different guided wave modes generated in a 1 mm-thick aluminum plate at 196 kHz using shearing line forces which was realized by applying the same in-plane pressure load (20 N) on all nodes of a line in the FEM simulation. In Fig. 3, the circumferential displacement $u_\theta$ denotes the $SH_0$ wave, the radial displacement $u_r$ denotes the $S_0$ wave and the out-of-plane displacement $u_z$ denotes the $A_0$ wave. It can be seen from Fig. 3(a) that a single shearing line force can excite $SH_0$ wave with the maximum amplitudes along 90° and 270° direction, and simultaneously excited Lamb waves ($S_0$ and $A_0$) with the maximum amplitudes along 0° and 180° direction. The ratio of the maximum $u_L$ ($u_r$ or $u_z$, whichever is larger) to maximum $u_\theta$, or abbreviated as LSR, is about 24% for the single line force of 12 mm length, and the half radiation angle θ of the excited $SH_0$ wave is about 65°. When two 12 mm-long antiparallel shearing line forces were employed, the LSR reduced to be within 10%, as seen in Fig. 3(b), which indicates that the antiparallel shearing line force is very effective in suppressing the Lamb waves. However, the radiation angle of the excited SH wave by the antiparallel line forces is just slightly smaller than that by single line force, indicating that the wave energy focusing function of the antiparallel line force is not significant.

When the length of the single line force increases to 24 mm, the LSR decreased to be about 16% and the half radiation angle θ decreases to be about 45°, as seen in Fig. 3(c). This indicates that increasing the length of the line force can also suppress the Lamb waves, but it is not as effective as the antiparallel line forces. Note that increasing the force length is very effective to focus the SH wave energy. In the case of antiparallel line forces of 24 mm length, the excited SLR further decreases to be about 6%, as seen in Fig. 3(d). As expected, the SH wave radiation angle almost keeps almost unchanged compared to that in Fig. 3(c).

### *3.2. Guided wave excitations by using single and antiparallel $d_{15}$ piezoelectric strips*

We further conducted the FEM simulations using the $d_{15}$ piezoelectric strips of the same length as the line forces in Fig. 3, and the results were shown in Fig. 4. Note that in all the cases, the strip width is 2 mm and the thickness is 0.8 mm. The piezoelectric materials used here is PZT-5H and its properties is listed in Table 1.

It can be seen from Fig. 4 that compared to the wave patterns generated by the shearing line forces in Fig. 3, the wave patterns generated by the 2 mm-wide, 0.8 mm-thick $d_{15}$ piezoelectric strips are

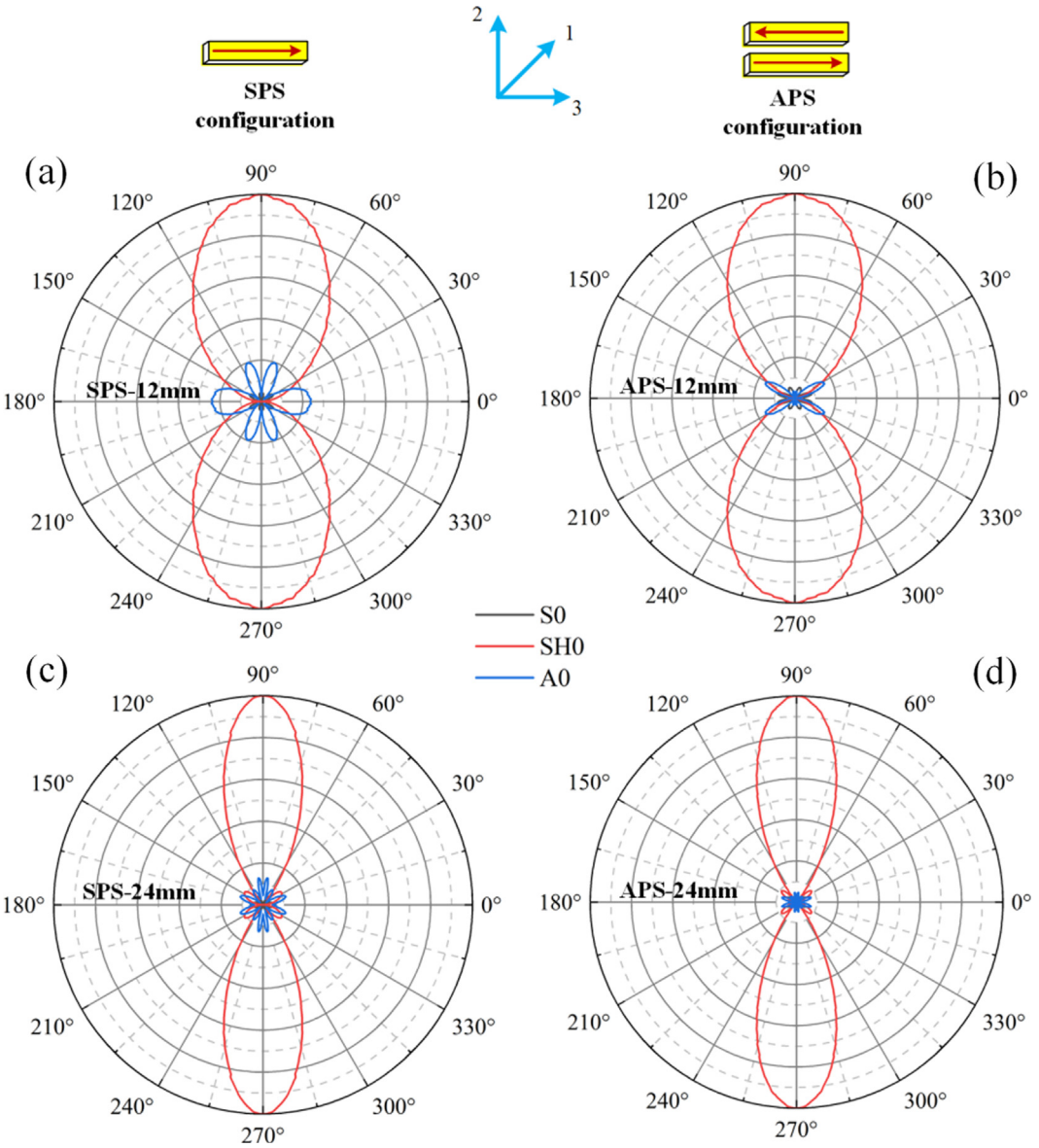


**Fig. 4.** Finite element simulated displacements of different guided wave modes generated in a 1 mm-thick aluminum plate at 196 kHz by using $d_{15}$ piezoelectric strips with the width of 2 mm and thickness of 0.8 mm. Left: Single piezoelectric strip of (a) 12 mm length (SPS-12 mm) and (c) 24 mm length (SPS-24 mm); Right: Antiparallel piezoelectric strips of (b) 12 mm length (APS-12 mm) and (d) 24 mm length (APS-24 mm). Interval between antiparallel piezoelectric strips is 8 mm.

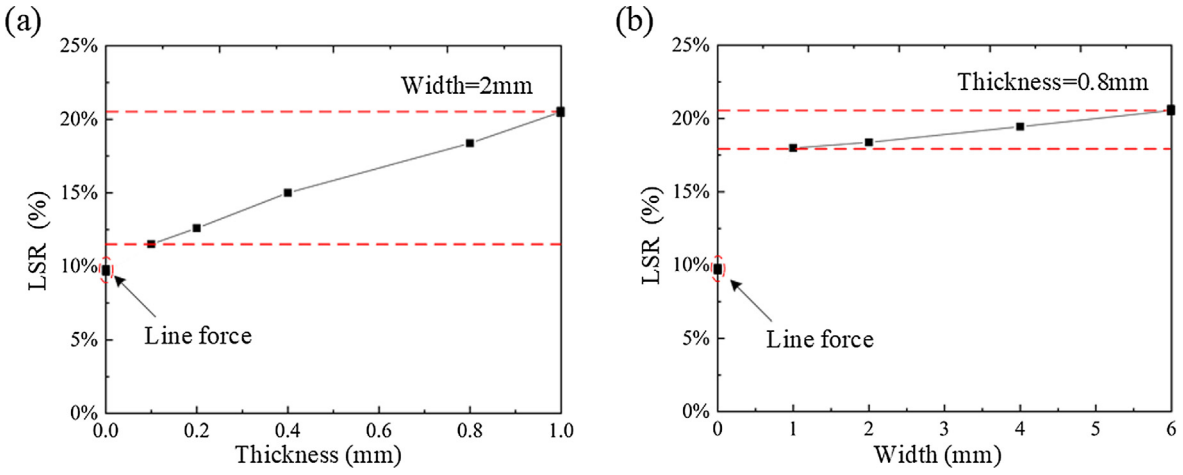


**Fig. 5.** Effect of strip thickness and width on the excited LSR (ratio of maximum Lamb wave displacement to maximum SH wave displacement) using antiparallel $d_{15}$ piezoelectric strips with the interval of 8 mm (working frequency 196 kHz). (a) Constant width of 2 mm; (b) constant thickness of 0.8 mm.

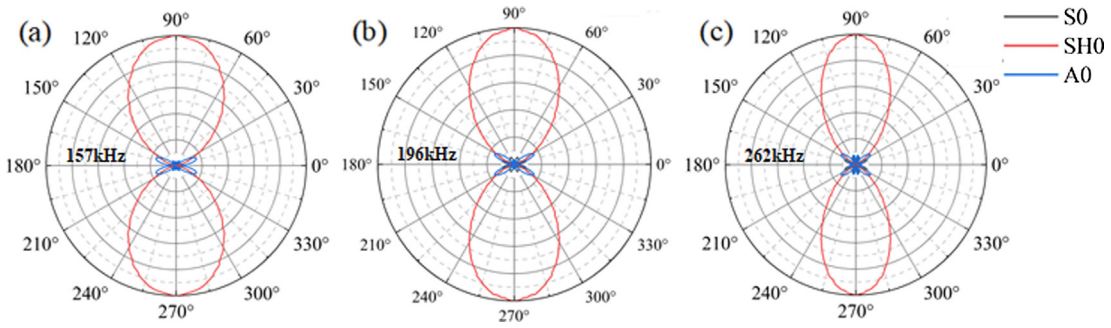


**Fig. 6.** FEM simulated guided wave patterns excited by using antiparallel 12 mm-long piezoelectric strips with different intervals (different exciting frequencies). (a) 10 mm, 157 kHz; (b) 8 mm, 196 kHz; (c) 6 mm, 262 kHz.

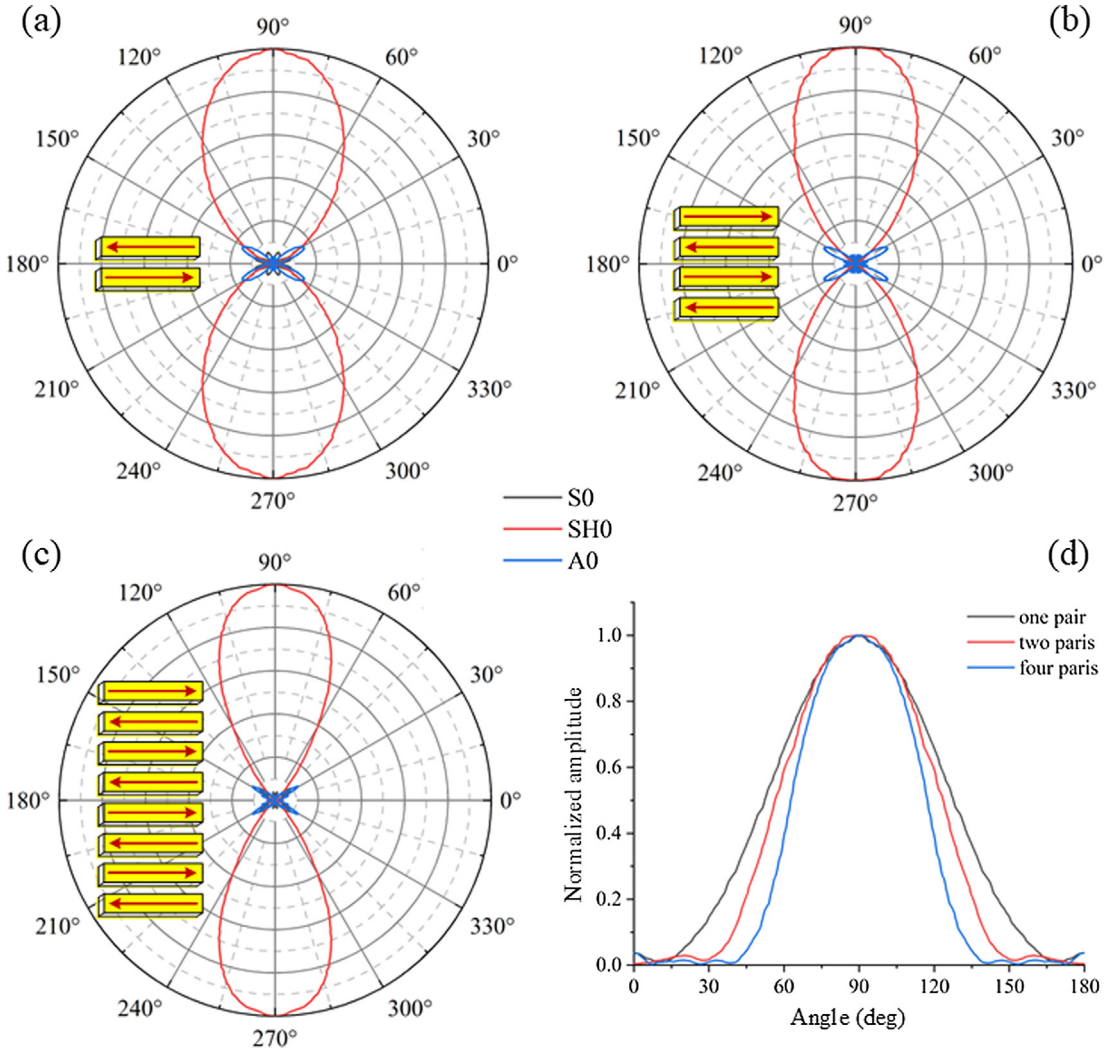


**Fig. 7.** FEM simulated wave patterns excited by using several pairs of 12 mm-long APS in one column. (a) One pair; (b) two pairs; (c) four pairs. (d) Radiation angles of excited $SH_0$ wave. Driving frequency of 196 kHz (strip interval of 8 mm).

similar. The excited LSR for the single piezoelectric strip case is very close to that for the single line force case, which is about 24% for the 12 mm-long strip and 16–17% for the 24 mm-long strip, as seen in Figs. 4(a) and 3(c). However, for the antiparallel piezoelectric strips cases in Fig. 4(b) and (d), the excited LSR is about 17% for the 12 mm length case and about 10% for the 24 mm length case, which are both larger than that of 10% and 6% by using the antiparallel line forces in Fig. 3(b) and (d). This may be due to the finite thickness and finite width of the piezoelectric strips, compared to the zero-thickness, zero-width line force. To examine the effect of strip thickness and strip width on suppressing the Lamb waves, we further conducted FEM simulations using piezoelectric strips of different thickness (constant width of 2 mm) and different widths (constant thickness of 0.8 mm), and the results were shown in Fig. 5.

It can be seen from Fig. 5(a) that at the constant width of 2 mm, the excited LSR using the APS increased steadily with the increasing thickness. However, at the constant thickness of 0.8 mm, the excited LSR just increased slightly with the increasing strip width, as seen in

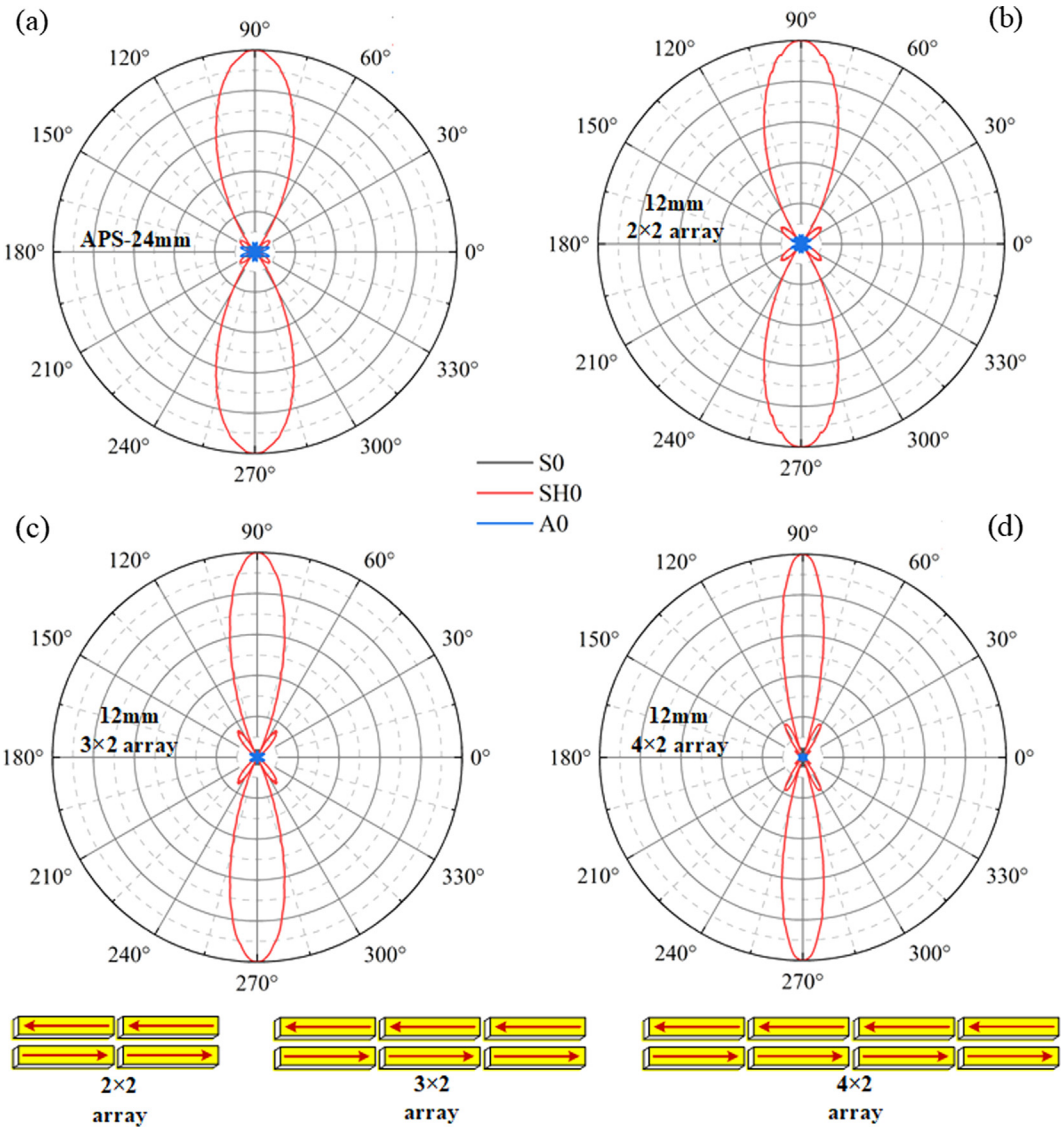


**Fig. 8.** FEM simulated wave patterns excited by using (a) one pair of 24 mm-long APS and 12 mm-long strips of (b) 2 × 2 array; (c) 3 × 2 array; (d) 4 × 2 array. Driving frequency is 196 kHz (strip interval of 8 mm).

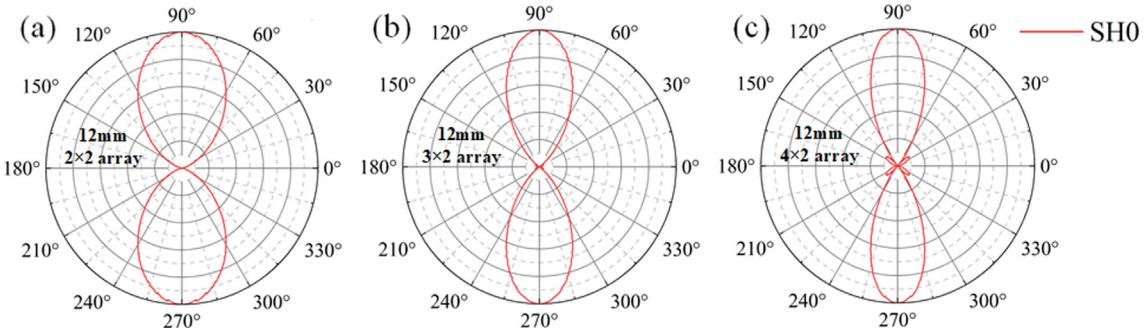


**Fig. 9.** FEM simulated $SH_0$ wave patterns excited by using 12 mm-long strips of (a) 2 × 2 array; (b) 3 × 2 array; (c) 4 × 2 array at 100 kHz (strip interval of 15.5 mm). Grating lobes of $SH_0$ were well suppressed.

Fig. 5(b). Therefore, the main differences of the excited LSR by using line forces and APS are due to the finite thickness of the APS. For a thicker strip, larger bending moment will be applied to the aluminum plate. In some directions, the bending moment induced by APS may be strengthened, leading to large grating lobes of the $A_0$ waves, as shown in Fig. 4(b).

### 3.3. Effect of strip interval (or driving frequency) of the APS

Fig. 6 shows the excited wave patterns by using one pair of 12 mm-long APS at different strip intervals of 10 mm, 8 mm and 6 mm, corresponding to driving frequencies of 157 kHz, 196 kHz and 262 kHz, respectively. It can be seen that with the increasing driving frequency, the

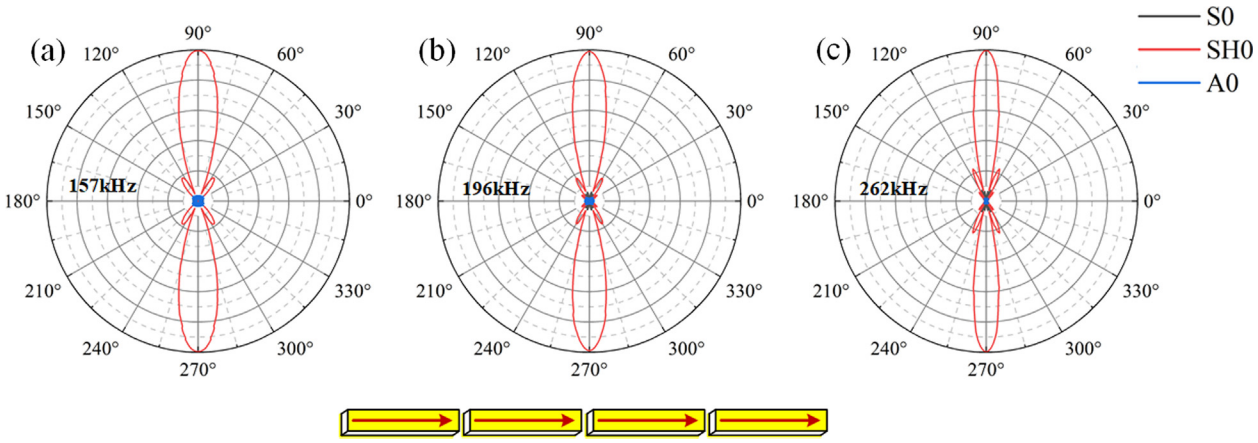


**Fig. 10.** FEM simulated guided wave patterns excited by using four 12 mm-long strips in one row at different frequencies: (a) 157 kHz; (b) 196 kHz; (c) 262 kHz.

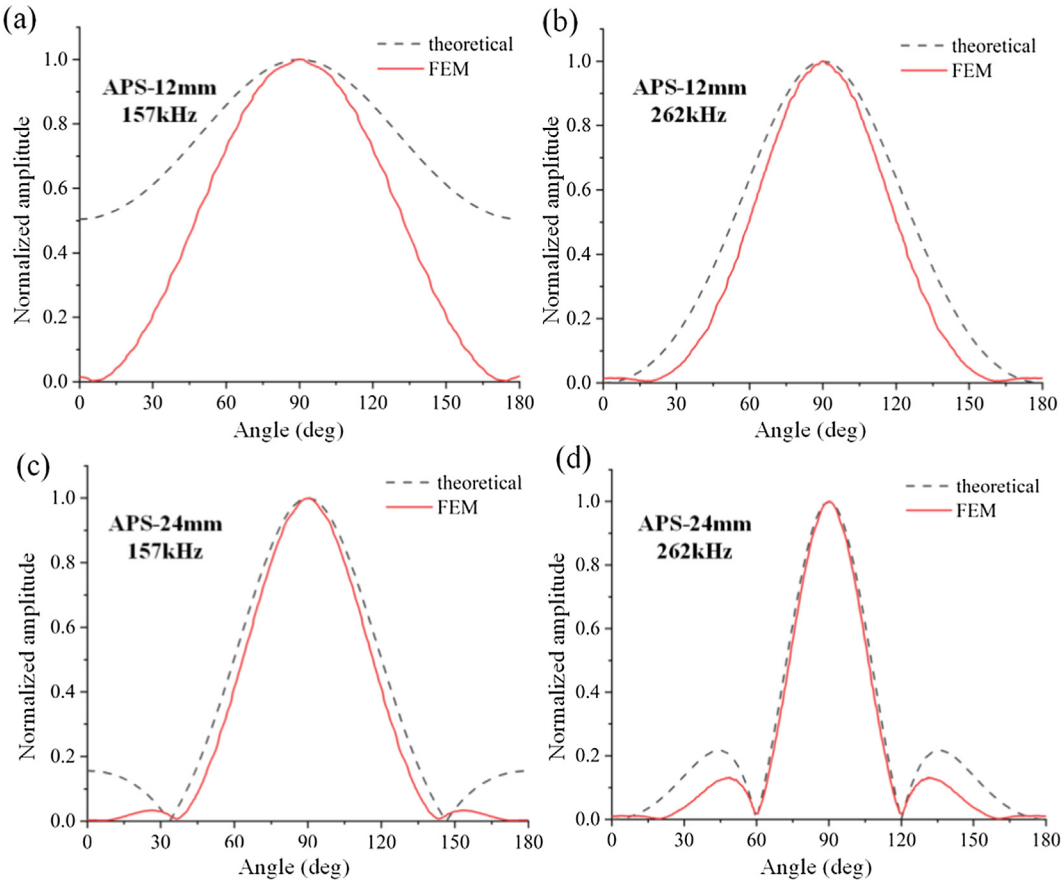


**Fig. 11.** The theoretical and simulated directivity function of $SH_0$ wave excited by using 12 mm-long APS (up) and 24 mm-long APS (bottom) under 157 kHz ($\lambda$ = 20 mm) and 262 kHz ($\lambda$ = 20 mm). The ratio $a/\lambda$ is 0.6, 1.0, 1.2 and 2.0 for (a), (b), (c) and (d), respectively.

excited LSR decreased steadily from 16.5% (157 kHz) to 13.6% (262 kHz), and the half radiation angle of the excited SH wave also decreased steadily, from about 65° to 55°. This indicates that increasing driving frequency (decreasing the strip interval) is quite effective in suppressing the Lamb waves and focusing the SH wave energy.

### 3.4. Performances of multiple pairs of antiparallel piezoelectric strips

We also studied the effect of more pairs of APS in one column, as in the case of PPM EMAT [6], on the excited SH wave. As seen in Fig. 7, the excited LSR decreased slowly with the increasing pairs of APS, it is 16.2% for one pair APS and 13.3% for the four pairs of APS case. As to the half radiation angle of SH wave, it decreases from about 75° (one pair APS) to about 50° (four pairs APS). That is, using more pairs of APS in one column would also suppress the Lamb waves and focus the SH wave energy, but the efficiency is much lower than that of using long strips. Therefore, in practical applications, it is not necessary to use more pairs of APS in one column.

Although increasing the strip length is very effective in suppressing the Lamb waves and focusing SH wave energy, in practice, long strips are difficult to pole and apt to break in applications. Here we proposed to synthesize a long strip using several short strips, that is, 2 × 2 array of 12 mm-long strips corresponds to a pair of 24 mm-long APS, 3 × 2 array corresponds to 36 mm-long APS and 4 × 2 array corresponds to

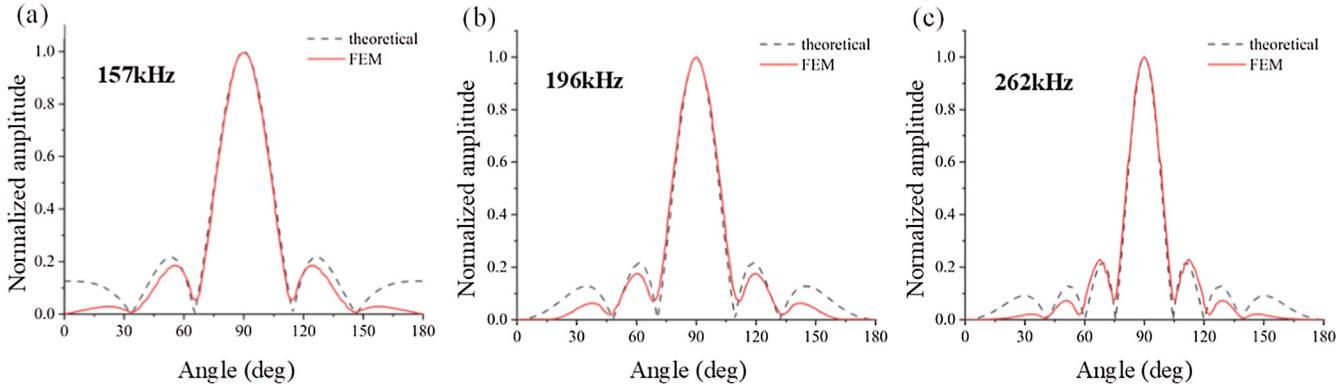


**Fig. 12.** The theoretical and simulated directivity function of $SH_0$ wave excited by using 12 mm-long strips 4 × 2 array under 157 kHz (λ = 20 mm), 196 kHz (λ = 16 mm) and 262 kHz (λ = 20 mm). The equivalent ratio $a/\lambda$ is 2.4, 3.0 and 4.0 for (a), (b) and (c), respectively.

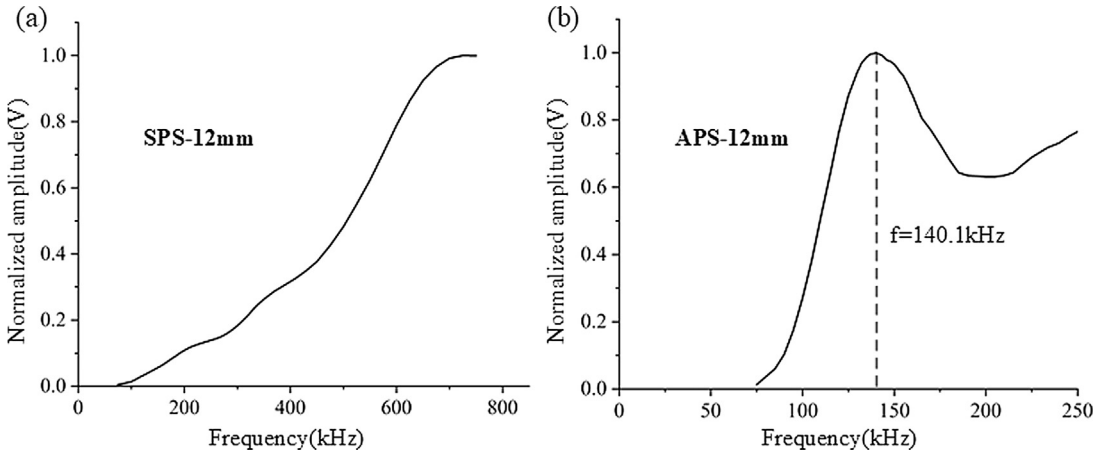


**Fig. 13.** Frequency dependent $SH_0$ wave excited by (a) a single 12 × 2 × 0.8 $mm^3$ $d_{15}$ piezoelectric strip and (b) antiparallel $d_{15}$ piezoelectric strips (APS) with the interval of 10 mm (nominal working frequency of 157 kHz). Another single $d_{15}$ piezoelectric strip placed at $90^0$ direction serves as the receiver.

48 mm-long APS. The simulated wave patterns using these arrays were shown in Fig. 8 where the results by 24 mm-long APS were also listed. It can be seen that the wave patterns excited by 2 × 2 array of 12 mm-long strips is almost identical to that by the 24 mm-long APS, i.e., the Lamb wave were well suppressed. But the grating lobes of $SH_0$ wave appeared in the 2 × 2 array case, which is 12.2% of the maximum $SH_0$ wave amplitude. In the case of the 3 × 2 array and 4 × 2 array, the Lamb waves were further suppressed while the grating lobes of $SH_0$ wave were enhanced to 15.7% and 18.3% of the maximum $SH_0$ wave amplitude. The grating lobes of $SH_0$ wave should be caused by the fact that the strip length (or column spacing) of 12 mm is larger than the half wavelength (8 mm) [41]. If the half wavelength is larger than 12 mm, the grating lobes should be well suppressed. This can be verified by the simulation results at 100 kHz (half wavelength of 15.5 mm), as seen in Fig. 9.

### 3.5. Performances of multiple piezoelectric strips in one row

We further simulated the performances of multiple $d_{15}$ piezoelectric strips in one row in generating guided waves since their performance should be almost equivalent to a very long $d_{15}$ strip, which can be inferred from Fig. 8. The advantage of using multiple strips in one row is that the working frequency can be varied freely in a wide range without reassembling the transducers. Fig. 10 shows the FEM simulated guided wave patterns excited by using four 12 mm-long $d_{15}$ PZT strips in one row at 157 kHz, 196 kHz and 262 kHz, respectively. It can be seen that at all frequencies, the Lamb waves were well suppressed with the LSR only about 5%. However, as expected, there appeared grating lobes of $SH_0$ wave with the amplitude about 20% of the main lobes. Meanwhile, the angle between the $SH_0$ grating lobes and the main lobes decreases steadily with the increasing frequency, which is about 40° at 157 kHz, 32° at 196 kHz and 25° at 262 kHz.

### 3.6. Comparison of theoretical and simulated $SH_0$ wave patterns excited by $d_{15}$ APS

From above simulations results, it can be seen that the radiation angles of the excited $SH_0$ wave using line forces and $d_{15}$ strips both decrease steadily with the increasing strip length and driving frequency. This tendency is very similar to the single-element bulk longitudinal wave radiation profile in the linear phased array system [42]. Since the $SH_0$ wave in plates is very similar to that of the bulk longitudinal wave in linear phased array systems, i.e., they are both non-dispersive and two-dimensional, we can anticipate that the theories for the latter may also be valid for the former.

Based on the bulk wave phased array theory [42], the far-field acoustic pressure excited by a single-element transducer with the width of $a$ is expressed by:

$$p(r, \theta, t) = \left(\frac{p_0}{r}\right)^{1/2} \frac{\sin(ka\sin\theta/2)}{k\sin\theta/2} \exp\left(-\frac{jka\sin\theta}{2}\right) \exp[j(\omega t - kr)] \quad (2)$$

where $p_0$ is the acoustic pressure at the center of the single-element transducer (here the geometry center of the $d_{15}$ APS). Note that here $\theta$ is the angle with respect to the main lobe direction, that is, $\theta = 0$ corresponds to the 90° direction or the main direction of the excited $SH_0$ wave. $k$ is the wave number, $\omega$ is the angular frequency and

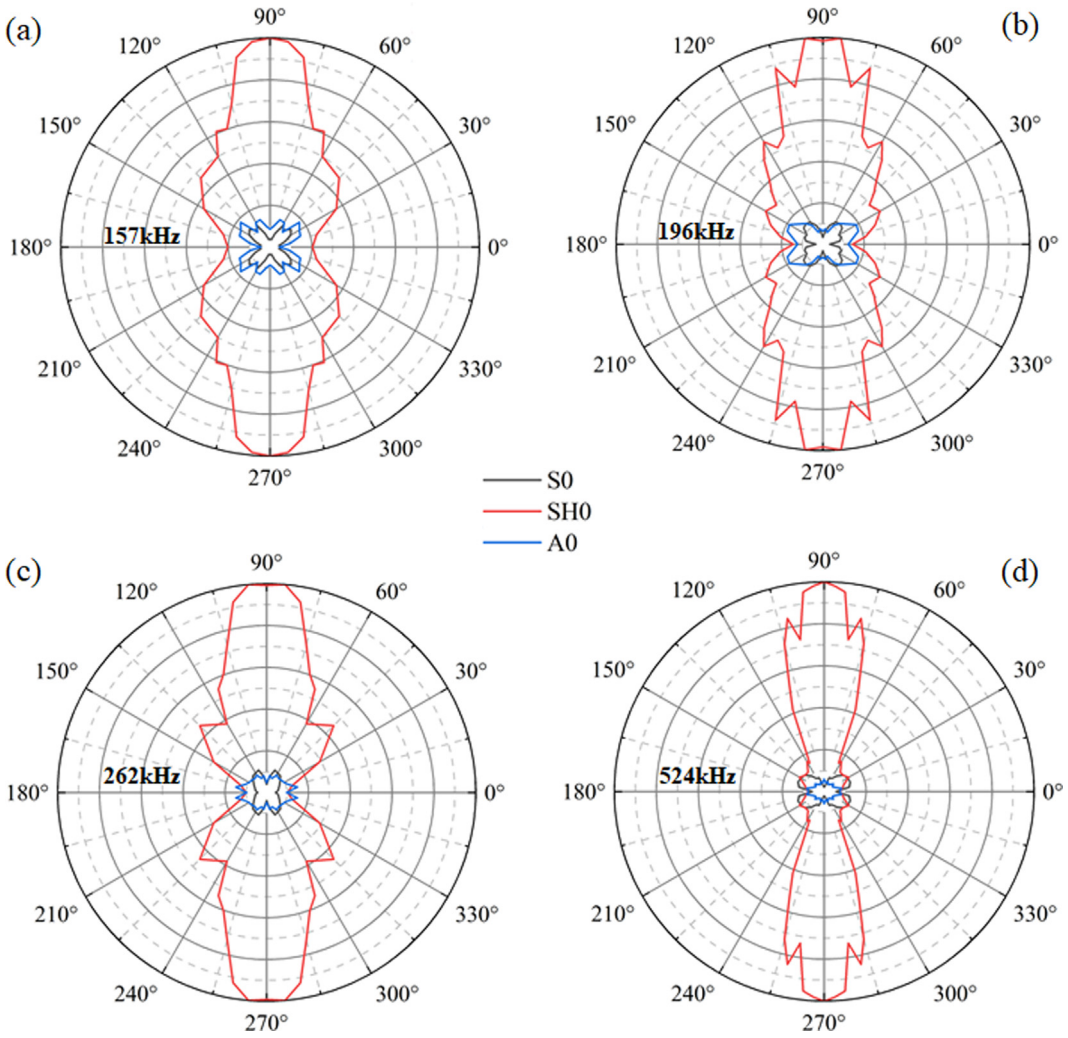


**Fig. 14.** Wave patterns excited by 12 mm-long APS with different intervals: (a) 10 mm (157 kHz); (b) 8 mm (196 kHz); (c) 6 mm (262 kHz); (d) 3 mm (524 kHz).

$$k = \frac{\omega}{c} = \frac{2\pi}{\lambda} \tag{3}$$

Here $c$ is the group velocity of the $SH_0$ wave, $\lambda$ is the wavelength corresponding to the central drive frequency.

The directivity function of the strip transducer is

$$H_1(\theta) = Q\left|\frac{\sin(ka\sin\theta/2)}{ka\sin\theta/2}\right| = Q\left|\frac{\sin(\pi a\sin\theta/\lambda)}{\pi a\sin\theta/\lambda}\right| \tag{4}$$

where Q is a constant or can be treated as unity.

Fig. 11 shows the theoretical (based on Eq. (4)) and FEM simulated directivity function of the $SH_0$ wave excited by 12 mm-long and 24 mm-long APS under 157 kHz ($\lambda$ = 20 mm) and 262 kHz ($\lambda$ = 20 mm), respectively. It can be seen from Fig. 11(a) that the theoretical curve cannot fit well with the simulated curve when $a/\lambda$ = 0.6. This is true because Eq. (4) can only describe bidirectional radiation profile when $a/\lambda \geq 1.0$ [42]. When this condition is satisfied, as seen in Fig. 11(b)–(d), the theoretical curve can fit well with the simulated curve. Furthermore, the larger $a/\lambda$, the better fit between the theoretical curves and simulated curves.

As indicated in Section 3.4, several $d_{15}$ strips in one row is almost equivalent to a very long strip in exciting SH wave, we further compare the theoretical and simulated directivity function of $SH_0$ wave excited by using 12 mm-long strips 4 × 2 array under 157 kHz, 196 kHz and 262 kHz with the equivalent $a/\lambda$ of 2.4, 3.0 and 4.0, and the results were shown in Fig. 12. It can be seen that in all the three cases, the theoretical curves fit almost perfectly with the simulated curves. This further confirmed that Eq.(4) can well predict the radiation profile of the $SH_0$ wave excited by $d_{15}$ strips when $a/\lambda > 1.0$, and the large $a/\lambda$, the better.

## 4. Experimental results

A series of experimental testing were then conducted to validate the designed bidirectional SH wave transducer. In all the testings, five-cycle sinusoid tone-burst signals with the applied voltage of 20 V were used to drive the bidirectional SH wave transducers.

### *4.1. Single-frequency property of the APS based bidirectional SH wave transducer*

Firstly, the SH wave excitation performances of a single 12 × 2 × 0.8 $mm^3$ $d_{15}$ piezoelectric strip and antiparallel $d_{15}$ piezoelectric strips (APS) with the interval of 10 mm (nominal working frequency of 157 kHz) were measured on a 1 mm-thick aluminum plate. Another 12 × 2 × 0.8 $mm^3$ $d_{15}$ strip bonded at $90^0$ direction with the distance of 360 mm from the exciter served as the SH wave receiver and the results were shown in Fig. 13. It can be seen that for the single $d_{15}$ strip, the amplitude of the excited $SH_0$ wave appeared at about 75 kHz and increased steadily with the frequency up to about 700 kHz. In comparison, the responses of the APS also appeared at about 75 kHz, it increased quickly with the frequency and reached a peak at about 140.1 kHz, which is close to the nominal working frequency of 157 kHz.

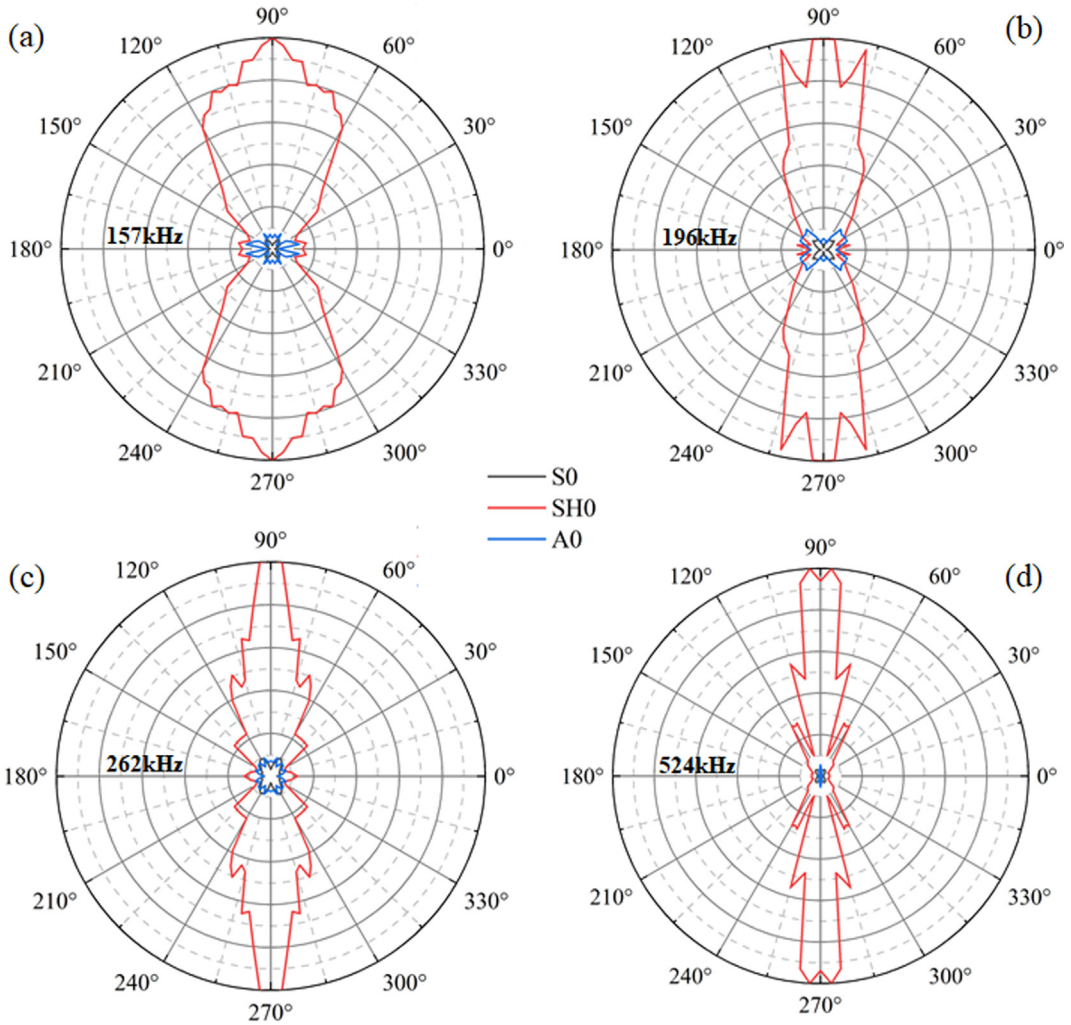


**Fig. 15.** Wave patterns excited by 20 mm-long APS with different intervals: (a) 10 mm (157 kHz); (b) 8 mm (196 kHz); (c) 6 mm (262 kHz); (d) 3 mm (524 kHz).

This confirmed that the designed bidirectional SH wave transducer is a single-frequency transducer. The discrepancy between the designed and actual working frequency, which is about 12%, may be due to the finite width (2 mm) of the piezoelectric strip or the mounting errors (the two strips may not be perfectly parallel), and such level of discrepancy can be acceptable in practice.

### *4.2. Wave patterns excited by the APS based bidirectional SH wave transducer*

Then, the wave patterns excited by 12 mm-long APS with different intervals (10 mm, 8 mm, 6 mm, 3 mm) were measured by using $d_{15}$ PZT strips (for receiving SH waves) and $d_{31}$ PZT disks (for receiving Lamb waves). Since the wave patterns were symmetric about the 0° direction and the 90° direction, measurements were only conducted from 0° to 90° and the results were shown in Fig. 14 in which the responses from other directions were obtained by mirroring. It should be noted that because the sensitivity of the $d_{15}$ PZT strip to $SH_0$ wave, and that of the $d_{31}$ PZT disk to $A_0$ wave and $S_0$ wave are different, and the three type sensitivities also vary with frequency, here for each wave mode, the sensitivities were calibrated using the maximum voltage amplitude and the FEM simulated maximum displacement in Fig. 6. For example, at 157 kHz, the maximum voltage amplitude received by the $d_{15}$ strip at 90° direction was 134.7 mV, then the relative sensitivity of the $d_{15}$ strip sensor at 157 kHz is 134.7 mV/unity since in all the simulations the displacement were normalized by the maximum $SH_0$ wave in-plane displacement at 90° direction. The maximum voltage amplitude corresponding to $A_0$ wave received by the $d_{31}$ sensor at 30° direction is 26.8 mV, and from Fig. 6(a) it can be seen that the relative displacement of $A_0$ wave along 30° is 0.17, then the relative sensitivity of the $d_{31}$ sensor to $A_0$ wave is 26.8/0.17 = 157.6 mV/unity. Similarly, the relative sensitivity of the $d_{31}$ sensor to $S_0$ wave can also be calibrated. With the sensor's relative sensitivity to all the three wave modes, the relative displacements can be straightforwardly obtained. For the 3 mm interval case (nominal frequency of 524 kHz) whose simulation results is lacking, the sensitivities for three wave modes were taken as the same as that for the 6 mm case (262 kHz).

It can be seen from Fig. 14 that consistent with the FEM simulation results in Fig. 6, the LSR excited by the APS is within 20% at 157 kHz and 196 kHz, and is within 15% at 262 kHz and 524 kHz. Overall, the half radiation angle of the excited $SH_0$ wave decreases with the increasing frequency, which is also consistent with the simulation results. The non-smooth wave patterns in Fig. 14 may be caused by the sensitivity variations between different SH wave and Lamb wave receivers.

Fig. 15 shows the excited wave patterns by using longer (20 mm) APS with different intervals of 10 mm (157 kHz), 8 mm(196 kHz), 6 mm (262 kHz) and 3 mm (524 kHz). It can be seen from Fig. 15 that consistent with the FEM simulation results in Fig. 4, longer APS resulted in smaller LSR, which is about 14% at 157 kHz, 12.6% at 196 kHz, 10% at 262 kHz and 6% at 524 kHz. Furthermore, the half radiation angle of excited bidirectional $SH_0$ wave using longer APS is also smaller than that using shorter ones, which is about 50° at 157 kHz, 40° at 196 kHz,

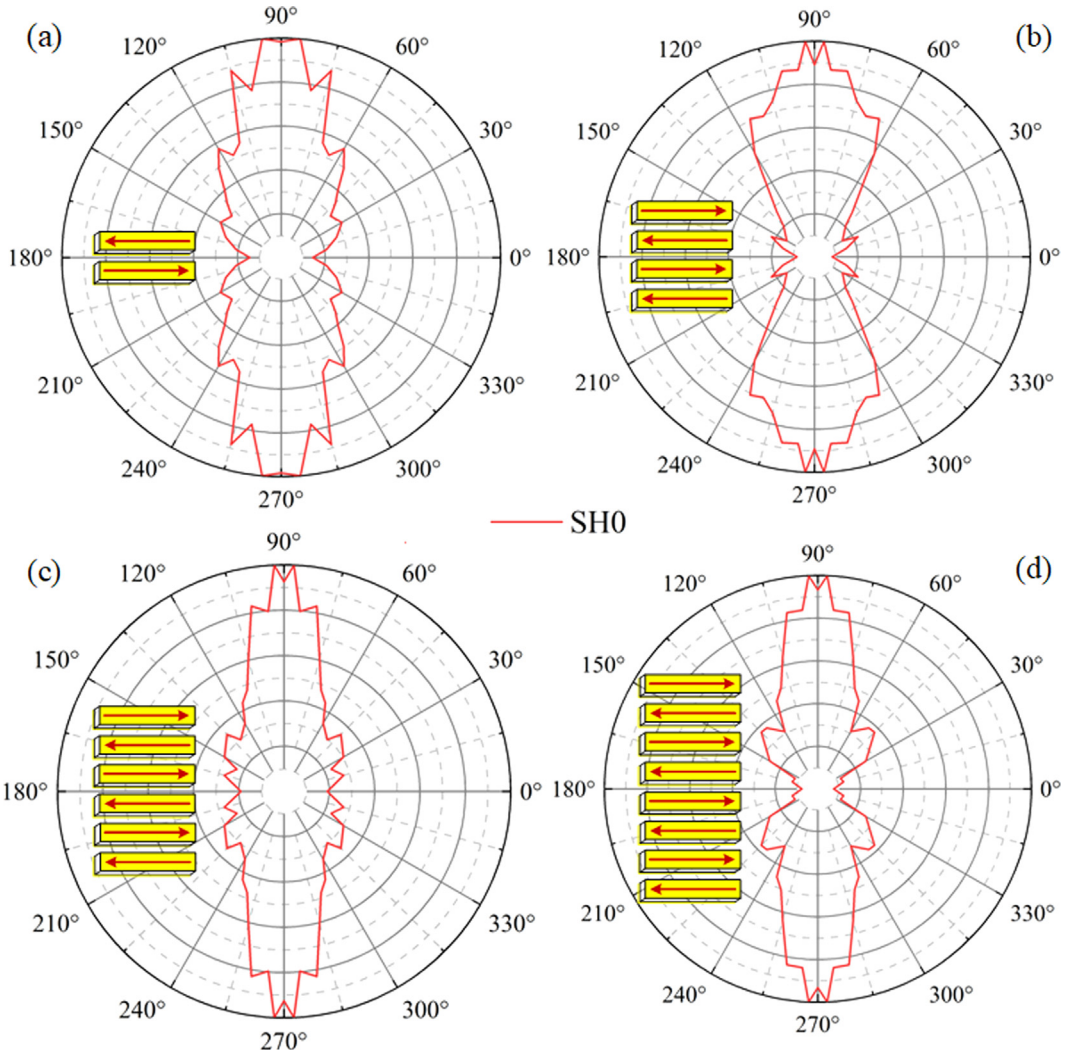


**Fig. 16.** $SH_0$ waves excited at 196 kHz (strip interval of 8 mm) by using several pairs of 12 mm-long APS in one column. (a) One pair; (b) two pairs; (c) three pairs. (d) four pairs.

30° at 262 kHz and 20° at 524 kHz. These results confirmed that longer APS is very effective in suppressing the Lamb waves and focusing SH wave. In addition, it can be seen from Fig. 15(d) that at 524 kHz, there appeared grating lobes of the excited $SH_0$ wave along the 60°, 120°, 240° and 300° directions, whose amplitude is about 28% of the maximum $SH_0$ wave amplitude along 90°. Therefore, it should be cautious when using very long strips at high frequency.

### 4.3. $SH_0$ wave excited by multiple pairs of APS

Fig. 16 shows the $SH_0$ waves excited by using several pairs of 12 mm-long APS in one column. It can be seen that consistent with the simulation results in Fig. 7, increasing the number of APS in one column can reduce the half radiation angle of excited $SH_0$ wave to some extent, but the efficiency is not high. Therefore, as stated in the simulation results in Section 3.4, it is not necessary to use more pairs of APS in one column.

Fig. 17 shows the excited $SH_0$ wave patterns by using 12 mm-long $d_{15}$ strips 2 × 2 array and 4 × 2 array at 262 kHz and 524 kHz, respectively. It can be seen that consistent with the FEM simulation results in Fig. 8, increasing the strip numbers along the row direction is almost equivalent to increasing the strip length, the excited $SH_0$ wave energy was greatly focused. The half radiation angle of the $SH_0$ wave for the 2 × 2 array case is about 30° at 262 kHz and about 20° at 524 kHz, while that for the 4 × 2 array case is only about 15° at 262 kHz and about 10° at 524 kHz. In Fig. 17, the experimental results at 262 kHz almost overlap the simulation results, and the experimental results at 524 kHz are also consistent with the theoretical curves, especially for the main lobe of the $SH_0$ wave. This indicated that the bidirectional SH wave radiation patterns excited by several $d_{15}$ strips can be well predicted using FEM simulations or theoretically. Therefore, in practice, to focus the excited SH wave energy, we can use more short $d_{15}$ piezoelectric strips in one row to synthesize very long strips. Meanwhile, increasing the driving frequency would further focus the wave energy and reduce the half radiation angle.

### 4.4. $SH_0$ wave excited by multiple $d_{15}$ piezoelectric strips in one row

We further examined the performances of four 12 mm-long $d_{15}$ strips in one row in excitation of SH waves at different frequencies and the results were shown in Fig. 18. It can be seen that consistent with the FEM simulation results in Fig. 10, the multiple strips in one row is almost equivalent to a very long strip, which can effectively focus the $SH_0$ wave energy. The half radiation angle of $SH_0$ wave decreases steadily with the increasing frequency, which is also consistent with the 4 × 2 strip array case in Fig. 17. The grating lobes of the excited $SH_0$ wave are also visible in Fig. 18, and their locations is also consistent with the simulation results in Fig. 10. At 524 kHz where the simulation result is

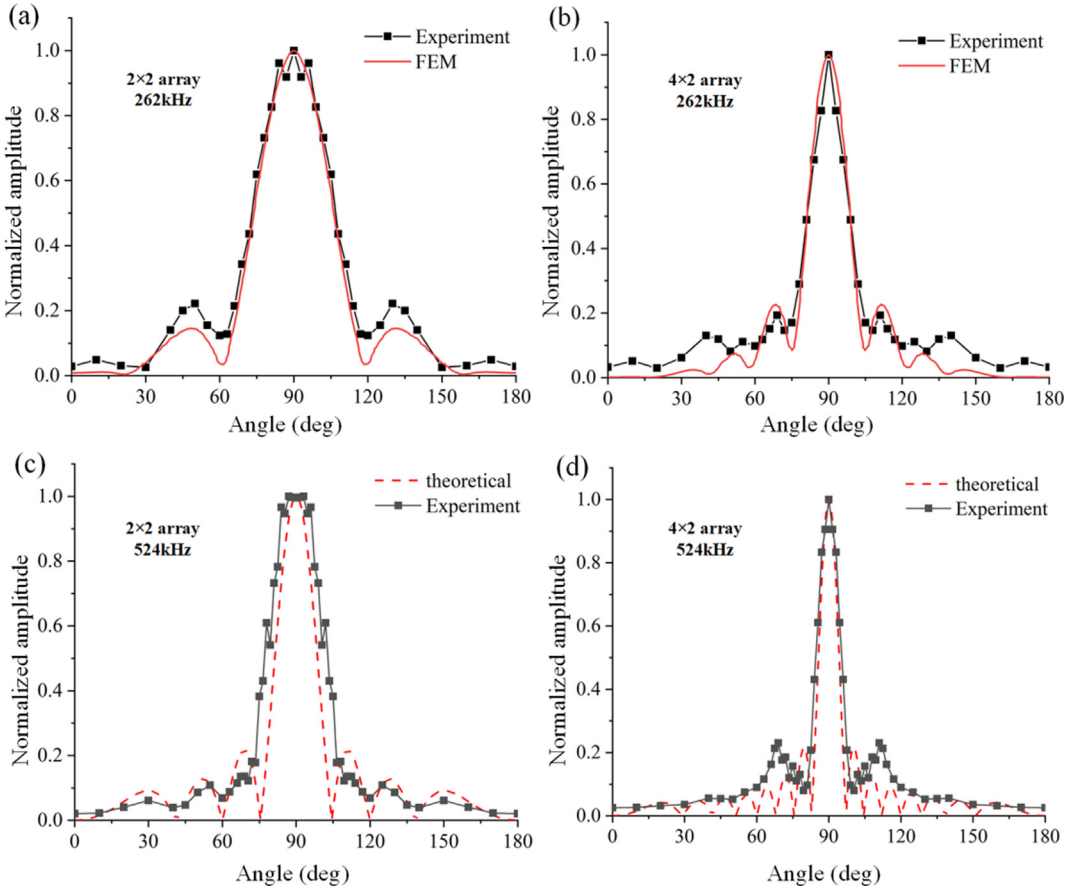


**Fig. 17.** The $SH_0$ wave radiation patterns excited by using 12 mm-long $d_{15}$ strips 2 × 2 array (left) and 4 × 2 array (right) at 262 kHz (up) and 524 kHz (bottom).

not available, the angle between the grating lobes and main lobes reduced to be only 13°, very close to the half radiation angle of about 10°. That is, at high frequency, the grating lobes can almost be negligible. As mentioned before, the advantage of using multiple strips in one row is that the working frequency can be varied freely.

### 4.5. Single-mode $SH_1$ wave excited by APS in a large *fd* plate

As indicated in Section 2.1, in large *fd*plates, to suppress the $SH_0$ wave and excite single-mode $SH_1$ wave, it is required that the strip interval $T = n\lambda_{SH0} \neq m\lambda_{SH1}$ (n, m are integers). Here we employed a thick aluminum plate with the dimensions of 1200 × 400 × 10 $mm^3$ as the wave guide in which the $SH_0$ wave velocity is calibrated to be 3010 m/s. Firstly, we select the condition of $T = \lambda_{SH0} = \frac{\lambda_{SH1}}{2}$ and it is deduced from Eq. (1) that $f_d$ = 1.74 MHz·mm, thus the driving frequency is selected as 174 kHz. From the group velocities curves of SH waves in the aluminum plate in Fig. 19, it can be seen that here the group velocity of $SH_1$ wave is 1523 m/s (Point A), which is much smaller than that of 3010 m/s for the $SH_0$ wave, thus they can be clearly identified in the time domain when a large travelling distance of 400 mm is used.

Fig. 20(a) shows the SH wave signals excited by using four 12 mm-long $d_{15}$ piezoelectric strip in one row at 174 kHz, from which it can be seen that both the $SH_0$ wave and $SH_1$ wave were clearly separated. Fig. 20(b) shows the SH wave signals excited by 12 mm-long APS 4 × 2 array with the interval of 17.3 mm (driving frequency 174 kHz), from which it can be seen that the $SH_0$ wave was well suppressed and the $SH_1$ wave was strengthened. However, the excited $SH_1$ wave at 174 kHz is strongly dispersive which can be explained by the dispersion curve in Fig. 19. At 160 kHz, the $SH_0$ wave were also well suppressed but the $SH_1$ wave seems not strengthened, seen in Fig. 20(c). As expected, at 200 kHz, the $SH_0$ wave were not well suppressed, as seen in Fig. 20(d).

We further excited single-mode $SH_1$ wave with weak dispersion, as denoted by Point B in Fig. 19. Here we employed the strip interval of $T = 2\lambda_{SH0}$ = 22 mm and the driving frequency of 273 kHz. From Eq. (1), it can be calculated that the group velocity of $SH_1$ wave at 273 kHz is 2513 m/s and the wavelength $\lambda_{SH1}$ = 9.2 mm, i.e., here $T = 2.4\lambda_{SH1}$ and the $SH_1$ wave should also be strengthened to some extent.

Fig. 21(a) shows the SH wave signals excited by using four 12 mm-long $d_{15}$ piezoelectric strip in one row at 273 kHz, from which it can be seen that the $SH_0$ wave and $SH_1$ wave can be just separated. When the APS 4 × 2 array were used, the excited $SH_0$ wave were well suppressed and the $SH_1$ wave were strengthened, as seen in Fig. 21(b). Furthermore, from Fig. 21(b), it can also be seen that the $SH_1$ wave excited at 273 kHz were only slightly dispersive, quite different from that excited at 174 kHz. As expected, at 210 kHz, the $SH_0$ wave were not suppressed and it can be clearly separated from the $SH_1$ wave, as shown in Fig. 21(c). At higher frequencies, see 330 kHz in Fig. 21(d), the $SH_0$ wave and $SH_1$ wave cannot be clearly separated because their group velocities is very close (3010 m/s vs. 2690 m/s). Thus, neither can be well suppressed or strengthened.

## 5. Discussions

From above simulation and experiments results, it can be seen that the $d_{15}$ APS can effectively excited bidirectional SH wave and suppress the Lamb wave. Its working frequency can be conveniently tuned by varing the interval between the strips. Compared with the PPM EMAT based SH wave transducer which requires a ~kW high-power driver [14–16], the APS based transducer proposed in this work can excited SH waves of large amplitude with the drive power less than 1 W (applied voltage typically of 20 V). Therefore, the proposed APS based SH

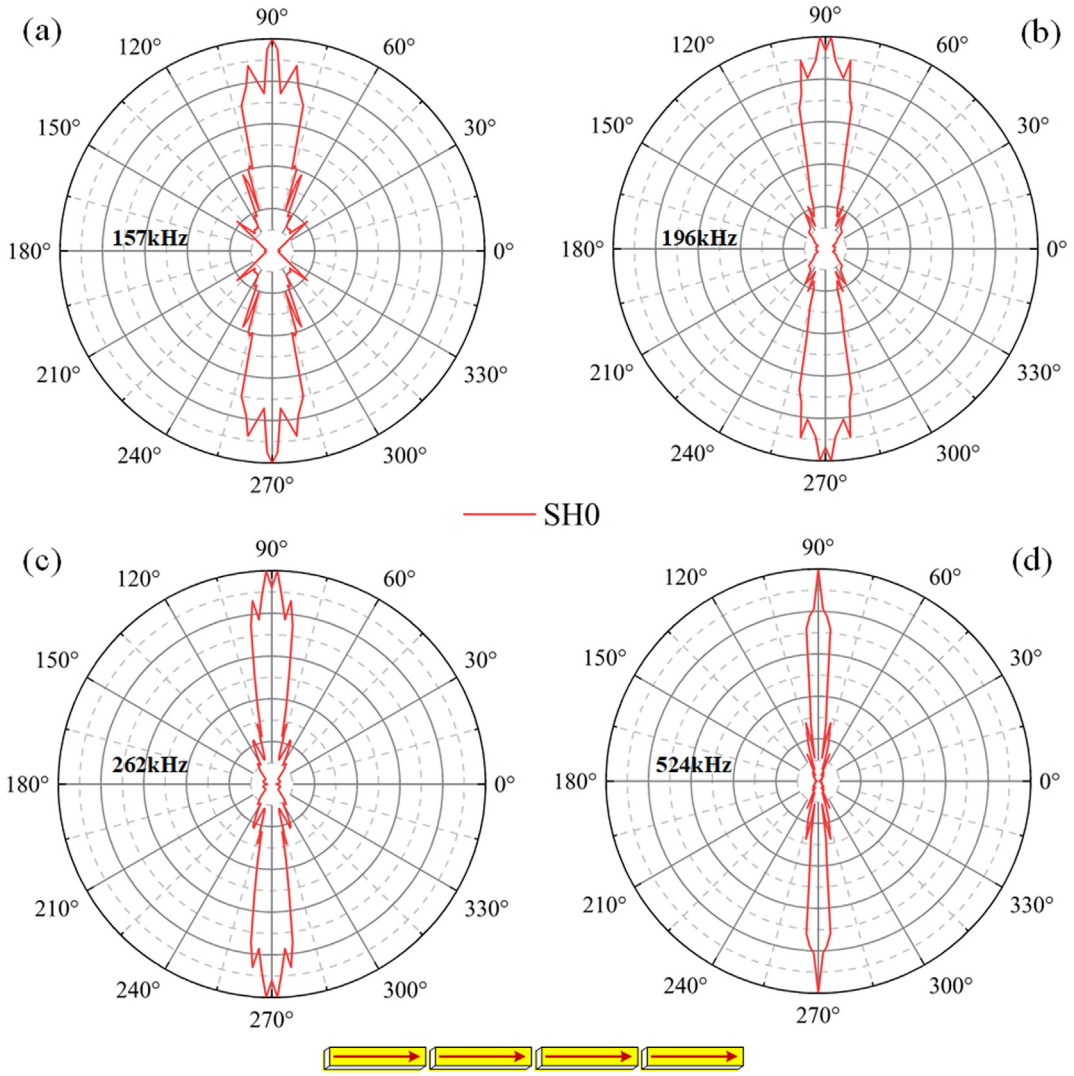


**Fig. 18.** $SH_0$ waves excited by using four 12 mm-long $d_{15}$ strips in one row at different frequencies: (a) 157 kHz; (b) 196 kHz; (c) 262 kHz; (d)524 kHz.

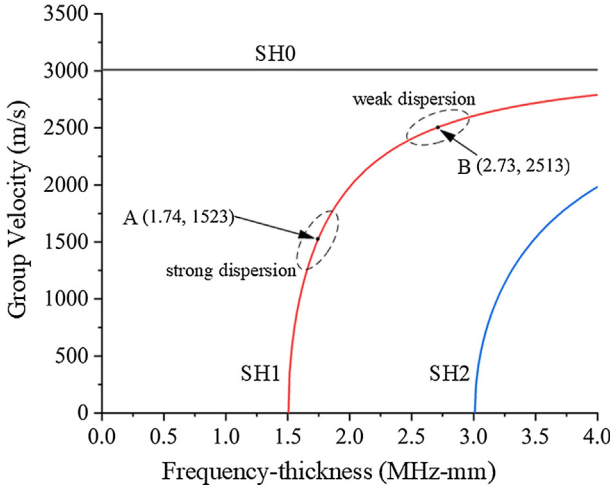


**Fig. 19.** The group velocities versus frequency-thickness product (*fd*) of first three order SH wave in a large aluminum plate.

wave transducer is expected to replace the EMAT based SH wave transducer when the contact mode is permitted.

The proposed thickness-shear $d_{15}$ APS bidirectional SH wave transducer is also superior to the bidirectional transducer based on dual face-shear $d_{24}$ piezoelectric wafers developed recently [24]. To change the working frequency, the $d_{15}$ APS transducer just needs to vary the strip intervals, while the dual-$d_{24}$ transducer is required to change the dimensions of the $d_{24}$ piezoelectric wafers. Meanwhile, the bandwidth of the $d_{15}$ strip (can reach up to 2 MHz when the thickness is below 0.5 mm) is considerably larger than that of the square $d_{24}$ wafer (typically below 300 kHz). In addition, the large-area electrode configuration of the $d_{15}$ strips is more convenient than the small-area electrode of the $d_{24}$ piezoelectric wafers.

## 6. Conclusions

In summary, we proposed a bidirectional SH wave transducer based on antiparallel $d_{15}$ piezoelectric strips (APS) whose working frequency can be easily tuned by varying the strip intervals. Both FEM simulations and experimental testing were conducted to validate the proposed bidirectional SH wave transducer. Results show that the excited Lamb waves by single $d_{15}$ piezoelectric strip can well be suppressed by increasing the strip length, reducing the strip interval (increasing drive frequency) or using more numbers of strips. The SH wave radiation angles can be fairly reduced using these measures. Meanwhile, it is found that using several short strips in a row is almost equivalent to a single long strip in excitation of SH waves. The proposed APS bidirectional transducer can also suppress the $SH_0$ wave and excite single-

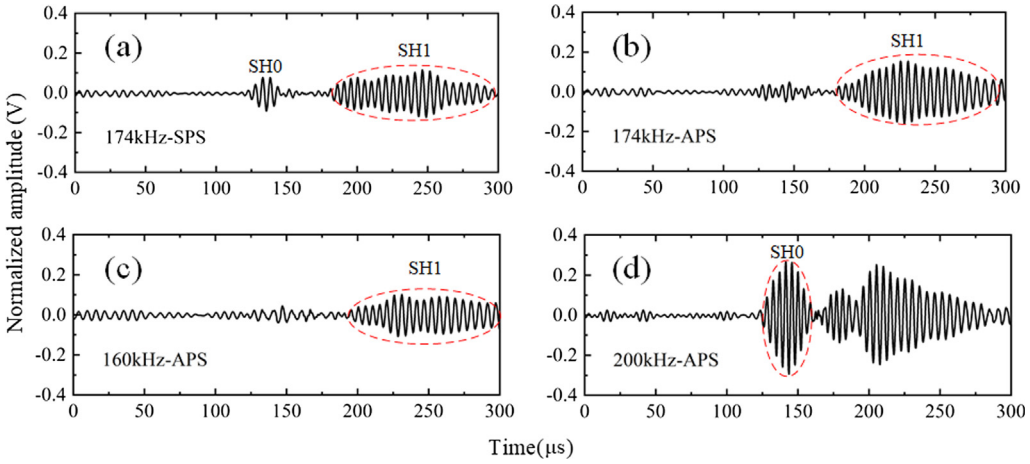


**Fig. 20.** Wave signals excited in a 1200 × 400 × 10 mm$^3$ aluminum plate by: (a) four single 12 mm-long piezoelectric strips in one row at 174 kHz; (b–d) 12 mm-long APS 4 × 2 array at 174 kHz, 160 kHz and 200 kHz. Signals received by a 12 mm-long $d_{15}$ strip 400 mm away from the exciter.

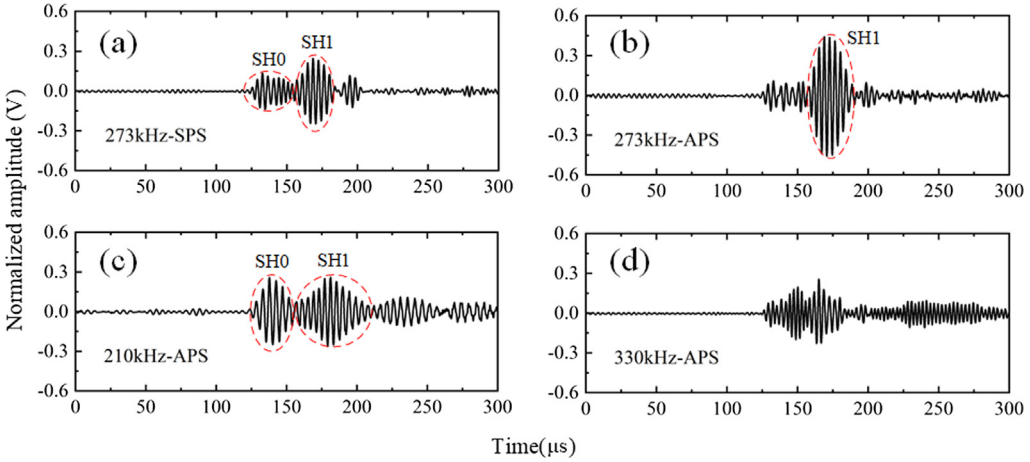


**Fig. 21.** Wave signals excited in a 1200 × 400 × 10 mm$^3$ aluminum plate by: (a) four single 12 mm-long piezoelectric strips in one row at 273 kHz; (b–d) 12 mm-long APS 4 × 2 array at 273 kHz, 210 kHz and 330 kHz. Signals received by a 12 mm-long $d_{15}$ strip 400 mm away from the exciter.

mode $SH_1$ wave in a large *fd* plate.

The proposed APS bidirectional SH wave transducer can be very useful in a variety of fields. (i) It can be used to excite bidirectional SH guided waves in plates, Love wave in a thin layer on a semi-infinite space and bulk SH waves in three-dimensional media, which are very essential to study the fundamental properties of SH waves, such as reflection, refraction, mode conversion, etc. (ii) It can be used to develop SH wave phase array system, SH wave tomography, etc. for defect locating and sizing in plates [43,44]. (iii) It can be used to excite circumferential SH waves for defect inspection in large-diameter pipelines. Due to its good performances, simple structure, tunable design and low cost, the proposed APS bidirectional SH wave transducer is expected to be widely used in above-mentioned areas.

## Acknowledgements

This work is supported by the National Natural Science Foundation of China under Grant Nos. 11672003 and 11890684.

## Appendix A. Supplementary material

Supplementary data to this article can be found online at https://doi.org/10.1016/j.ultras.2019.06.001.

## References

[1] F.-K. Chang, Structural Health Monitoring 2000, CRC Press, 1999.
[2] D. Alleyne, B. Pavlakovic, M. Lowe, P. Cawley, Rapid, long range inspection of chemical plant pipework using guided waves, in: AIP, 2001, pp. 180–187.
[3] Z. Su, L. Ye, Y. Lu, Guided Lamb waves for identification of damage in composite structures: a review, J. Sound Vib. 295 (2006) 753–780.
[4] V. Giurgiutiu, Structural Health Monitoring: With Piezoelectric Wafer Active Sensors, Elsevier, 2007.
[5] J.L. Rose, Ultrasonic Waves in Solid Media, Cambridge University Press, 2004.
[6] C. Vasile, R. Thompson, Excitation of horizontally polarized shear elastic waves by electromagnetic transducers with periodic permanent magnets, J. Appl. Phys. 50 (1979) 2583–2588.
[7] R.B. Thompson, Generation of horizontally polarized shear waves in ferromagnetic materials using magnetostrictively coupled meander-coil electromagnetic transducers, Appl. Phys. Lett. 34 (1979) 175–177.
[8] H. Kwun, C.M. Teller, Magnetostrictive generation and detection of longitudinal, torsional, and flexural waves in a steel rod, J. Acoust. Soc. Am. 96 (1994) 1202–1204.
[9] H. Kwun, I.C.M. Teller, Nondestructive evaluation of non-ferromagnetic materials using magnetostrictively induced acoustic/ultrasonic waves and magnetostrictively detected acoustic emissions, 1995.
[10] Y.Y. Kim, C.I. Park, S.H. Cho, S.W. Han, Torsional wave experiments with a new magnetostrictive transducer configuration, J. Acoust. Soc. Am. 117 (2005) 3459–3468.
[11] S.H. Cho, S.W. Han, C.I. Park, Y.Y. Kim, Noncontact torsional wave transduction in a rotating shaft using oblique magnetostrictive strips, J. Appl. Phys. 100 (2006) 104903.
[12] H.M. Seung, H.W. Kim, Y.Y. Kim, Development of an omni-directional shear-horizontal wave magnetostrictive patch transducer for plates, Ultrasonics 53 (2013) 1304–1308.
[13] Y.Y. Kim, Y.E. Kwon, Review of magnetostrictive patch transducers and applications in ultrasonic nondestructive testing of waveguides, Ultrasonics 62 (2015)

3–19.
[14] R. Ribichini, F. Cegla, P.B. Nagy, P. Cawley, Study and comparison of different EMAT configurations for SH wave inspection, IEEE Trans. Ultrason. Ferroelectr. Freq. Control. 58 (2011) 2571–2581.
[15] N. Nakamura, H. Ogi, M. Hirao, K. Nakahata, Mode conversion behavior of SH guided wave in a tapered plate, NDT E Int. 45 (2012) 156–161.
[16] P. Petcher, S. Dixon, Mode mixing in shear horizontal ultrasonic guided waves, Nondestruct. Test. Eval. 32 (2017) 113–132.
[17] M. Castaings, SH ultrasonic guided waves for the evaluation of interfacial adhesion, Ultrasonics 54 (2014) 1760–1775.
[18] Z. Wei, S. Huang, S. Wang, W. Zhao, Magnetostriction-based omni-directional guided wave transducer for high-accuracy tomography of steel plate defects, IEEE Sens. J. 15 (2015) 6549–6558.
[19] Z. Liu, X. Zhong, M. Xie, X. Liu, C. He, B. Wu, Damage imaging in composite plate by using double-turn coil omnidirectional shear-horizontal wave magnetostrictive patch transducer array, Adv. Compos. Mater. 26 (2017) 67–78.
[20] P. Wilcox, M. Lowe, P. Cawley, Lamb and SH wave transducer arrays for the inspection of large areas of thick plates, in: AIP, 2000, pp. 1049–1056.
[21] G. Boivin, M. Viens, P. Belanger, Plane wave SH0 piezoceramic transduction optimized using geometrical parameters, Sensors 18 (2018) 542.
[22] H. Miao, Q. Huan, F. Li, Excitation and reception of pure shear horizontal waves by using face-shear d24 mode piezoelectric wafers, Smart Mater. Struct. 25 (2016) 11LT01.
[23] Q. Huan, H. Miao, F. Li, Generation and reception of shear horizontal waves using the synthetic face-shear mode of a thickness-poled piezoelectric wafer, Ultrasonics 86 (2018) 20–27.
[24] H. Miao, Q. Huan, F. Li, G. Kang, A variable-frequency bidirectional shear horizontal (SH) wave transducer based on dual face-shear (d24) piezoelectric wafers, Ultrasonics 89 (2018) 13–21.
[25] P. Belanger, G. Boivin, Development of a low frequency omnidirectional piezoelectric shear horizontal wave transducer, Smart Mater. Struct. 25 (2016) 045024.
[26] H. Miao, Q. Huan, Q. Wang, F. Li, A new omnidirectional shear horizontal wave transducer using face-shear (d24) piezoelectric ring array, Ultrasonics 74 (2017) 167–173.
[27] Q. Huan, H. Miao, F. Li, A uniform-sensitivity omnidirectional shear-horizontal (SH) wave transducer based on a thickness poled, thickness-shear (d15) piezoelectric ring, Smart Mater. Struct. 26 (2017) 08LT01.
[28] Q. Huan, M. Chen, F. Li, A practical omni-directional SH wave transducer for structural health monitoring based on two thickness-poled piezoelectric half-rings, Ultrasonics (2018).
[29] M. Ratassepp, M. Lowe, P. Cawley, A. Klauson, Scattering of the fundamental shear horizontal mode in a plate when incident at a through crack aligned in the propagation direction of the mode, J. Acoust. Soc. Am. 124 (2008) 2873–2882.
[30] P. Rajagopal, M. Lowe, Scattering of the fundamental shear horizontal guided wave by a part-thickness crack in an isotropic plate, J. Acoust. Soc. Am. 124 (2008) 2895–2904.
[31] P. Belanger, High order shear horizontal modes for minimum remnant thickness, Ultrasonics 54 (2014) 1078–1087.
[32] N. Nazeer, M. Ratassepp, Z. Fan, Damage detection in bent plates using shear horizontal guided waves, Ultrasonics 75 (2017) 155–163.
[33] X. Yu, M. Ratassepp, Z. Fan, Damage detection in quasi-isotropic composite bends using ultrasonic feature guided waves, Compos. Sci. Technol. 141 (2017) 120–129.
[34] Q. Huan, H. Miao, F. Li, A variable-frequency structural health monitoring system based on omnidirectional shear horizontal wave piezoelectric transducers, Smart Mater. Struct. 27 (2018) 025008.
[35] Q. Huan, M.T. Chen, F.X. Li, A high-resolution structural health monitoring system based on SH wave piezoelectric transducers phased array, Ultrasonics (2019), https://doi.org/10.1016/j.ultras.2019.04.005.
[36] P. Li, S. Shan, F. Wen, L. Cheng, A fully-coupled dynamic model for the fundamental shear horizontal wave generation in a PZT activated SHM system, Mech. Syst. Signal Process. 116 (2019) 916–932.
[37] G. Liu, J. Qu, Guided circumferential waves in a circular annulus, J. Appl. Mech. 65 (1998) 424–430.
[38] X. Zhao, J.L. Rose, Guided circumferential shear horizontal waves in an isotropic hollow cylinder, J. Acoust. Soc. Am. 115 (2004) 1912–1916.
[39] P. Wilcox, M. Lowe, P. Cawley, Omnidirectional guided wave inspection of large metallic plate structures using an EMAT array, IEEE Trans. Ultrason. Ferroelectr. Freq. Control. 52 (2005) 653–665.
[40] Q. Huan, M. Chen, F. Li, A comparative study of three types shear mode piezoelectric wafers in shear horizontal wave generation and reception, Sensors 18 (2018) 2681.
[41] B.W. Drinkwater, P.D. Wilcox, Ultrasonic arrays for non-destructive evaluation: a review, NDT E Int. 39 (2006) 525–541.
[42] S.-C. Wooh, Y. Shi, Optimum beam steering of linear phased arrays, Wave Motion 29 (1999) 245–265.
[43] J. Rao, M. Ratassepp, Z. Fan, Limited-view ultrasonic guided wave tomography using an adaptive regularization method, J. Appl. Phys. 120 (19) (2016) 194902.
[44] J. Rao, M. Ratassepp, D. Lisevych, M. Hamzah Caffoor, Z. Fan, On-line corrosion monitoring of plate structures based on guided wave tomography using piezoelectric sensors, Sensors 17 (12) (2017) 2882.